Journal of the European Ceramic Society **10** (1992) 143–150

Interaction Between Crack Deflection and Crack Bridging

Jürgen Rödel

Technische Universität Hamburg–Harburg, Advanced Ceramics Group, W-2100 Hamburg 90, Germany

(Received 9 December 1991; revised version received 6 April 1992; accepted 6 May 1992)

Abstract

The potential of crack deflection and crack bridging as competing toughening mechanisms is reviewed. Available measurement techniques take a crucial role where it is required to distinguish between toughening increments associated with crack tip processes and crack wake processes near the crack tip. Particular emphasis is placed on measurements of the crack opening displacement. It is concluded that crack deflection has only small potential as a toughening mechanism compared to crack bridging, but is required to activate crack closure stresses associated with bridging ligaments. This simple realization defines a window of microstructural parameters in which crack deflection is active and where crack bridging parameters can be optimized.

Rißablenkung und Rißüberbrückung werden als konkurrierende bruchzähigkeitserhöhende Mechanismen untersucht. Eine Schlüsselrolle nehmen dabei die derzeit verfügbaren Meßmethoden ein. Diese dienen vor allem zur Ermittlung von Bruchzähigkeitssteigerungen, die auf Prozesse an der Rißspitze und den Rißflanken nahe der Rißspitze zurückgeführt werden können. Besonders wichtig sind dabei Messungen der Rißöffnung. Die Ergebnisse zeigen, daß Rißablenkung im Vergleich zur Rißüberbrückung nur ein kleines Potential zur Erhöhung der Bruchzähigkeit besitzt—aber entscheidend für die Bildung von Schließspannungen ist. Die Gefügeparameter müssen deshalb so eingestellt werden, daß Rißablenkung möglich ist. Dann kann der Effekt der Rißüberbrückung optimiert werden.

Cet article examine le potentiel respectif de la déviation et du pontage des fissures en tant que mécanisms concurrents permettant d'augmenter la ténacité. Les techniques de mesures disponibles jouent un rôle crucial pour différencier l'augmentation de la ténacité associée à la propagation de la fissure proprement dite des mécanismes survenant dans le sillage de celle-ci. Nous concluons que la déviation de fissure joue un rôle mineur par rapport au pontage des fissures, mais cela demande d'induire des contraintes visant à refermer la fissure grâce aux éléments de pontage. Cette simple étude permet la définition d'une gamme de paramètres microstructuraux pour laquelle la déviation des fissures joue un rôle actif et où le pontage de ces dernières peut être optimisé.

1 Introduction

About 15 years ago, a renewed interest in structural ceramics culminated in a fundamental recognition: ceramics can be manufactured with a crack resistance which represents more than the energy absorbed when two fracture surfaces separate irreversibly in a brittle matrix. Processing methods, theoretical modeling efforts and mechanical characterization techniques were developed, all in the quest to produce tougher ceramics. From the very beginning, however, it appeared difficult to ascertain what the major toughening mechanisms are and could be; hence which are the material characteristics to be improved. If transformation toughening[1] is left aside as a now well-understood phenomenon, it is found that the discussion centers around two questions: Is microcrack toughening[2] or crack bridging[3] the dominant toughening mechanism for a class of materials containing residual stresses (e.g. $Al_2O_3^4$)? Is crack deflection[5] or crack bridging[3] the dominant toughening mechanism for a class of materials containing elongated particles (e.g. silicon carbide whisker-reinforced alumina or Si_3N_4)? Note

Journal of the European Ceramic Society 0955-2219/92/$5.00

that the following question is contained implicitly: what is the toughening mechanism in a material containing both residual stresses and elongated particles?

Here the author attempts to provide a perspective for the second question. Crack deflection is defined as the twist and tilt of the crack front between microstructural elements which leads to an increase of fracture toughness at the crack tip. Crack bridging is described as the process where microstructural elements connect both crack faces and transmit a closure force across the crack walls, which—by definition—occurs behind the crack tip and leads to a crack-length dependent fracture toughness (R-curve).

The discussion is begun by following the evolution of the understanding of both crack deflection and crack bridging over the last 15 years. This will include theoretical as well as experimental approaches. Since crack deflection is a mechanism active at the crack tip and crack bridging is a mechanism active in the crack wake, the measurement techniques will be particularly emphasized and new characterization methods based on an evaluation of the crack opening displacement will be discussed. Two case studies, on silicon carbide whisker-reinforced alumina ($SiC(w)/Al_2O_3$) and Si_3N_4, will be used to test the present understanding.

2 Fracture Mechanics

To set the scene, a brief description of the relevant fracture mechanics principles is given.

The author will resort to two approaches, connected with either the stress intensity factor concept or the strain energy release rate concept.

Stress intensity factors are additive quantities. In equilibrium, the applied stress intensity factor K_A is balanced by a crack-length dependent fracture toughness $K_R(c)$, being composed of a crack tip toughness T_0 (which is affected by crack deflection) and a term $T_\mu(c)$, which arises due to closure stresses in the crack wake (crack bridging).

$$K_A = K_R(c) = T_0 + T_\mu(c) \tag{1}$$

The shielding term $T_\mu(c)$ can be represented through an appropriate integration over all closure stresses $\delta(t)$ active in the crack wake. For the case of an embedded penny crack (Fig. 1), the shielding term is obtained as follows[6] (s, t are parameters describing the source points where closure stresses are active).

$$T_\mu(c) = 2/(\pi c)^{1/2} \int_0^c (t\delta(t)\,\mathrm{d}t)/(c^2 - t^2)^{1/2} \tag{2}$$

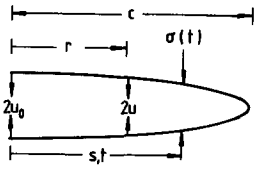

Fig. 1. Schematic giving the geometric parameters if looking down into the bottom right side of an embedded penny crack configuration.

This description includes the crack length c as scaling parameter, but, since $\delta(t)$ is a function of crack geometry, sample geometry and stress field, eqn (2) fails to provide a satisfactory physical basis.

A more fundamental computation is afforded if the J-integral formulation[7] is used, which is based on an energy concept. The mechanical energy release rate, J, is balanced by a crack tip energy term R_0 and a shielding term $R_\mu(u_0)$:

$$J = R(u_0) = R_0 + R_\mu(u_0) \tag{3}$$

The shielding term $R_\mu(u_0)$ is obtained by integrating over the closure forces stored or dissipated in the crack wake up to a maximum crack opening u_0 (at the last bridge):

$$R_\mu(u_0) = 2\int_0^{u_0} p(u)\,\mathrm{d}u \tag{4}$$

Here p is the average closure stress in the crack wake as a function of crack opening $2u$ (Fig. 1). The crack profile (u as $f(r)$) is determined by the Sneddon double integral equation[8] (eqn (5)) and provides a means of relating the parameters in the stress intensity factor concept (eqns (1) and (2)) to the parameters in the energy-based approach (eqns (3) and (4)).

$$u(r) = 4/\pi E' \int_r^c \mathrm{d}s/(s^2 - r^2)^{1/2} \int_0^s \delta(t)t\,\mathrm{d}t/(s^2 - t^2)^{1/2} \tag{5}$$

3 Chronology

In the following some key papers in the literature are referred to which accelerated the learning process in the discussion of crack deflection and crack bridging in ceramics.

3.1 Crack deflection

In 1975 Borom *et al.*[9] considered crack deflection as an energy absorbing mechanism. Specifically, it was used to explain the strength of abraded glass ceramics containing elongated Li_2Si_{05} crystals in the matrix.

In 1983 two key papers by Faber & Evans[5,10] set

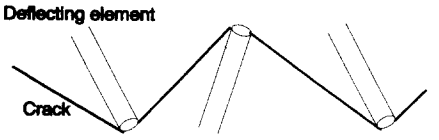

Fig. 2. Mechanism of crack deflection (after Faber & Evans[5]).

the standard for crack deflection processes (see Fig. 2). The theoretical analysis incorporated effects due to volume fraction of second-phase particles, particle morphology and aspect ratio as well as the distribution of interparticle spacing. Particles with rod-shaped morphology are predicted to be most suitable for maximizing toughening. The companion paper[10] was conceived to provide experimental verification for the theoretical predictions. A glass ceramic with lath-shaped $Li_2Si_2O_5$ crystals (the same material as studied by Borom *et al.*[9]) and a Si_3N_4 with rod-shaped grains were the focus of this investigation. The experimental data (toughness, crack deflection profiles and crack deflection angle) appeared to strengthen the case made in the theoretical study: a toughness increase is viable through inclusion of second-phase particles, particularly rod-shaped particles with large aspect ratio. Looking at both papers with the benefit of seeing the field mature for a further eight years, it can be noted that: (1) the micrographs of cracks in the lithium aluminosilicate glass ceramic, shown to demonstrate crack deflection, give prime examples for elastic and elastic–plastic bridging elements. Therefore, at least part of the toughness increase (if not most) in these materials is due to crack bridging; (2) high-toughness Si_3N_4 with rod-shaped grain morphology is now known to show *R*-curve behavior (see later case studies), that is, crack wake and not solely crack tip processes are effective.

In 1990, in a review by Evans[11] on the development of high-toughness ceramics, a number of toughening mechanisms are reviewed, but crack deflection is not included anymore. In contrast, Evans noted that all tough ceramics exhibit *R*-curve behavior, placing the emphasis on crack wake mechanisms.

In 1991, in an article on microstructural design of toughened ceramics, Becher[12] considers toughening mechanisms, particularly as afforded by incorporation of whiskers into the matrix material. Again, crack deflection is only briefly mentioned, but crack bridging is discussed in detail.

3.2 Crack bridging

In 1978 the relatively high fracture toughness of Si_3N_4 containing rod-shaped grains was explained by Lange[13] as being a consequence of fibre pull-out. The frictional energy dissipated while elongated grains slide out of their respective sockets was added to the critical strain energy release rate of the matrix material.

In the same year *R*-curve behavior was reported for alumina by Hübner & Jillek.[14] The authors surmised that an interference between the fracture surfaces should lead to additional energy consumption due to friction. Unfortunately the observations made in this paper had no immediate impact.

In 1982 a very pertinent observation came from Knehans & Steinbrech,[15] who reported that *R*-curves are observed in alumina, but are geometry dependent. In their classical 'saw-cut experiment' they demonstrated that the increase in crack resistance with crack length is associated with crack wake phenomena.

In 1985 optical observations of interacting crack faces (in Al_2O_3), again by Knehans & Steinbrech,[16] provided definite proof for the crack bridging mechanism. This approach was later extended by Swanson *et al.*[17] (1987) and Swanson[18] (1988).

In 1989, in-situ SEM studies of equilibrium cracks in various ceramic materials[19] sharpened the picture gained through optical microscopy alone. Similar studies are now performed routinely.[20,21] SEM studies also provide the opportunity to quantify closure stresses in the crack wake through a measurement of the crack opening displacement.[21] Finally, a classification scheme[22] for various types of crack bridges exists. In this context, Fig. 3 shows micrographic examples of various bridge categories. It supplements the classification scheme given earlier[22] by including ductile bridges, in addition to the categories afforded by brittle elements (elastic, plastic and elastic–plastic bridges).

4 Measurement

4.1 Established measurement techniques

The difficulty in establishing the effectiveness of crack deflection versus crack bridging in increasing the fracture toughness of a given material in part reflects a deficiency in reliable fracture toughness measurement techniques. In principle, one only needs to apply eqns (1) and (2) and provide for a crack geometry, such that $T_\mu(c) \ll T_0$. This requirement appears satisfied if c is very small. Therefore one simply needs to measure the toughness of very short cracks.

In practice, experimental limitations obtain, in general associated with the length or opening of a pop-in starter crack, in detail related to the

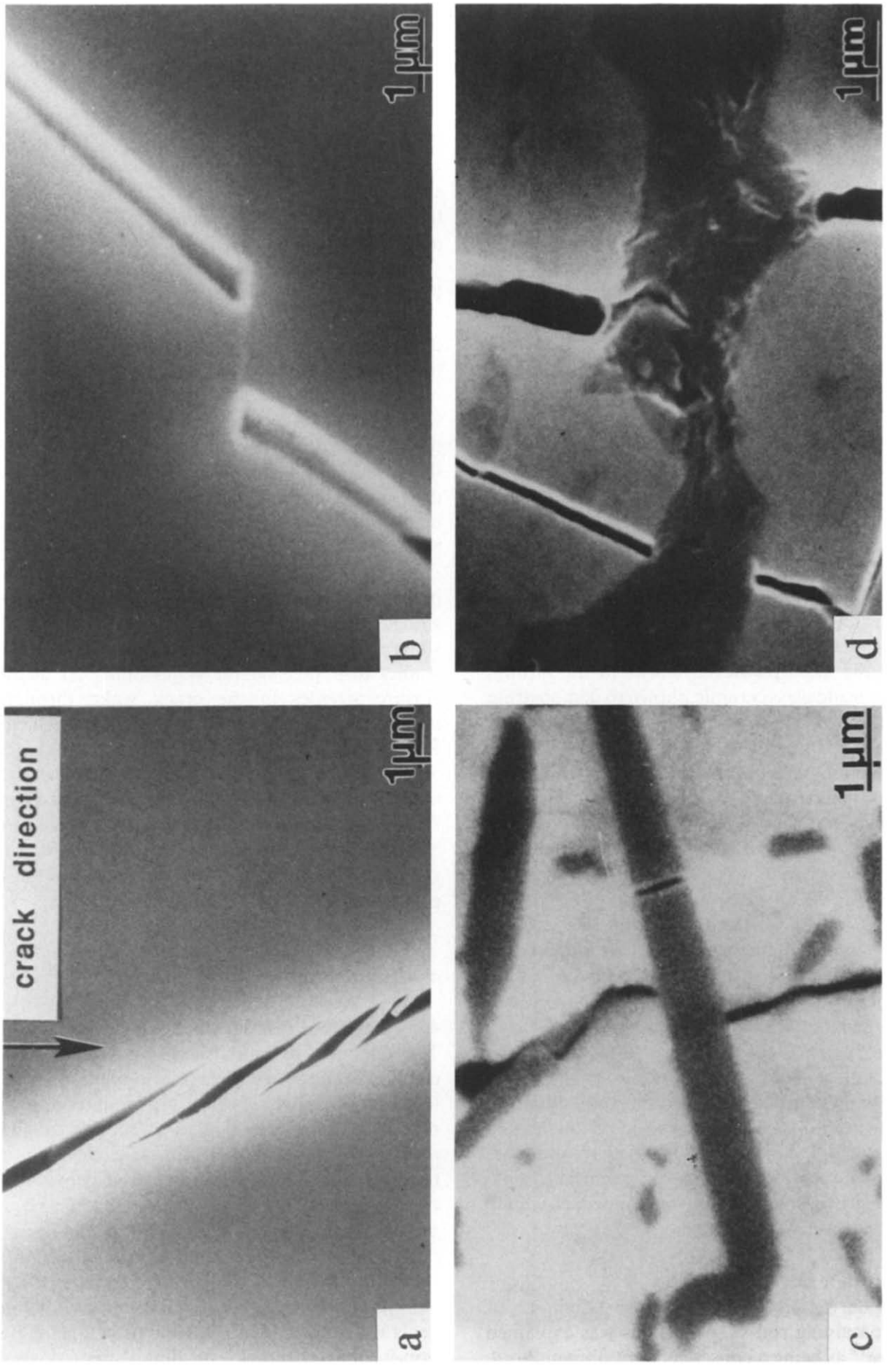

Fig. 3. Representative examples for (a) elastic bridges (distance from the crack tip, $x = 410\,\mu m$; SiC grain: $Al/Al_2O_3/SiC$ composite), (b) plastic bridge ($x = 290\,\mu m$; Al_2O_3), (c) elastic/plastic bridge ($x = 100\,\mu m$; $SiC(w)/Al_2O_3$) and (d) ductile bridge ($x = 360\,\mu m$; $Al/Al_2O_3/SiC$). Cracks run from top to bottom.

particular crack geometry chosen. Straight-through cracks, surface cracks and indentation cracks will be discussed.

Straight cracks in a CT (compact tension) or DCB (double cantilever beam) specimen require a starter crack of about 100–200 μm length to guarantee that the crack is continuous between the sample surfaces. These cracks are too long, however, to provide fracture toughness values if the question is concerned with strength of materials and fracture toughness associated with failure causing defects. Even more importantly, these cracks cannot distinguish between crack bridging in the first 100–200 μm behind the crack tip and crack deflection at the crack tip.

Surface cracks can be accompanied by a residual stress field (which provide a 'local criterion' for crack initiation). This leads to an additional K-term through an appropriate integration as exemplified in eqn (2). If this term is not known, eqn (1) is incomplete and cannot be used to evaluate the crack tip toughness T_0 or the shielding term $T_\mu(c)$.

Radial indentation cracks with their residual stress field defined by the elastic–plastic contact zone are a further alternative for the measurement of fracture toughness of short cracks. The limitations of eqns (1) and (2), however, become apparent in this case. More than a short crack, a narrow crack (small u_0) is now required to determine the crack tip related fracture toughness. This is more plausible in considering eqn (3) in conjunction with eqn (4). The shielding term contribution to the crack resistance is kept minimal if the crack opening at the last active bridge is kept small. Exactly this requirement is violated in radial indentation cracks. The large residual stresses centered at the edge of the contact zone, lead to a relatively (compared to crack length) large energy consumption by separating the crack faces to a value u_0 as specified by the residual stress field, the bridging stresses and the applied stress field. A complete discussion of this complex topic is beyond the scope of this paper and is given elsewhere.[23] For the present purposes it is sufficient to note that radial indentation cracks are characterized by relatively (compared to residual stress-free surface cracks) large crack opening displacements. These in turn lead to a relatively large energy consumption during crack propagation. This situation is illustrated in Fig. 4 for a material free of bridging tractions (soda lime glass). The peak opening of a radial indentation crack is about four times higher than the COD as predicted for a surface crack. Finally, it should not be misconstrued that eqns (1) and (2) alone are insufficient to describe the

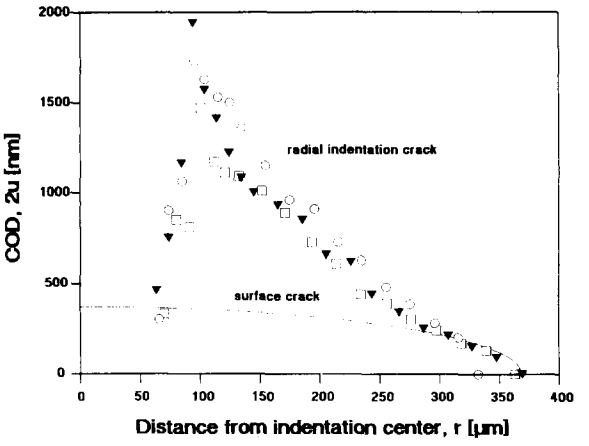

Fig. 4. Crack opening displacement data for radial indentation crack (indentation load = 78 N) in glass and theoretical predictions for residual stress-free surface crack (full line); elastic–plastic contact zone half-diameter is 80 μm.

fracture toughness as measured by radial indentation cracks; eqn (4), however, provides immediate physical insight.

4.2 New measurement opportunities

New, fundamental ways of measuring the crack tip fracture toughness T_0 are illustrated by use of Fig. 5. In a material without R-curve the linear elastic crack tip stress field is given by:

$$\delta_y = K_y/(2\pi r)^{1/2} f(\theta) \tag{6}$$

with δ_y the tensile component of the stress field. Raman spectroscopy has recently been employed to measure the elastic stresses in front of the crack tip.[24] The crack opening displacement $u(x)$ has the form:

$$u(x) = (8x/\pi)^{1/2} K_I/E' \tag{7}$$

with x, r, θ defined as in Fig. 5. In principle, measurement of either quantity, stress field ahead of the crack tip or crack opening displacement behind the crack tip, allow computation of T_0 for equilibrium cracks. In practice, eqn (7) appears more appealing, compared to eqn (6), since a geometrical parameter (width between crack faces) can be measured. For the case of a bridged crack, with the bridging zone small compared to crack and sample

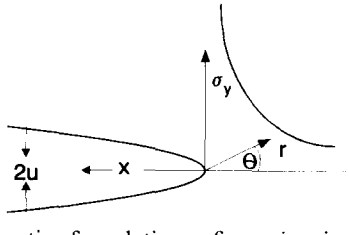

Fig. 5. Schematic of crack tip configuration, including crack tip stress field and COD.

dimensions, eqn (7) has to be modified[21] to yield:

$$u(x) = (8x/\pi)^{1/2} K_{tip}/E' + 4/\pi E' \int_0^c p(x')\{(x/x')^{1/2} - \tfrac{1}{2}\ln[|(x'^{1/2}+x^{1/2})/(x'^{1/2}-x^{1/2})]|\}\,dx' \quad (8)$$

Here x denotes the field point, where the COD is evaluated, and x' the source point where closure stresses are acting; both parameters, x and x', are written as a distance from the crack tip. Solving for K_{tip}, eqn (9) is obtained:

$$K_{tip} = u(x)E'(\pi/8x)^{1/2} - (2/\pi x)^{1/2} \int_0^c p(x') \times \{(x/x')^{1/2} - \tfrac{1}{2}\ln[|(x'^{1/2}+x^{1/2})/(x'^{1/2}-x^{1/2})]|\}\,dx' \quad (9)$$

In practice, COD measurements are only possible at a distance of about 10 μm to the crack tip. These measurements have been performed and, by neglecting the integral term, gave an estimate for K_{tip} in Al_2O_3,[21] whisker-reinforced Al_2O_3,[25] and metal reinforced Al_2O_3.[26]

Here a mathematical analysis of the accuracy of this method is provided. To do so, eqn (9) is rewritten as eqn (10):

$$K_{tip} = u(x)E'(\pi/8x)^{1/2} - K_f \quad (10)$$

with K_f from eqn (11):

$$K_f = (2/\pi x)^{1/2} \int_0^c p(x') \times \{(x/x')^{1/2} - \tfrac{1}{2}\ln[|(x'^{1/2}+x^{1/2})/(x'^{1/2}-x^{1/2})]|\}\,dx' \quad (11)$$

An upper bound for K_f is obtained by replacing $p(x')$ through the maximum of the occurring closure stresses, p_m (eqn (12)):

$$K_f < K_f' = (2/\pi x)^{1/2} p_m \int_0^c \times \{(x/x')^{1/2} - \tfrac{1}{2}\ln[|(x'^{1/2}+x^{1/2})/(x'^{1/2}-x^{1/2})]|\}\,dx' \quad (12)$$

This procedure is only allowed if the integrand essentially does not change sign, which was verified for this case. Analytical integration of eqn (12) yields eqn (13):

$$K_f' = (2/\pi x)^{1/2} p_m \int_0^c \{(x-x') - \ln[|(x'^{1/2}+x^{1/2})/(x'^{1/2}-x^{1/2})]|\} + 2(xx')^{1/2} \quad (13)$$

K_f as well as K_f' are now essentially determined by x and p_m. Taking the values obtained for Al_2O_3,[21] $p_m = 70$ MPa, $x = 10\,\mu$m and taking a distance over which closure stresses are acting from $x = 0$ to $x = 1900\,\mu$m as the area of integration, $K_f < 0{\cdot}02$ MPa $\sqrt{m}$. Now K_f gives a definite, mathematically defined uncertainty value for the crack tip toughness determination by measurement of the near crack tip opening displacement. It is, however, considerably below the experimentally related uncertainty, which enters the K_{tip} determination, since the COD near the crack tip cannot be obtained accurately. This uncertainty amounts to a value in K_{tip} of about 0·5 MPa $\sqrt{m}$. In practice, COD measurements at a distance of about 10 μm to the crack tip therefore allow a determination of K_{tip} (and T_0) with an accuracy of about 20–30%.

5 Case Studies

The crack deflection–crack bridging argument is central in the discussion on the toughening mechanism of two material classes: silicon carbide whisker-reinforced alumina and Si_3N_4, containing rod-shaped grains. In the following succinct descriptions of the current understanding of both ceramics are given.

5.1 SiC(w)/Al_2O_3

Long crack fracture toughness measurements[27] demonstrated the existence of an R-curve in this material, with the lowest toughness values at 5·6 MPa $\sqrt{m}$. Subsequent measurements from crack growth studies and fracture strength determinations of indented specimens[28–30] reinforced the notion of a rising crack resistance with crack length in this material. The accessible crack length regime is shifted down to a starting value of 50 μm, with corresponding fracture toughness values[28] $K_R >$ 5 MPa $\sqrt{m}$.

Values obtained using the indentation crack length as a fracture toughness indicator[30] are in the region $K_R > 4{\cdot}5$ MPa $\sqrt{m}$ for $c > 30\,\mu$m. Comparatively large radial indentation cracks[29] (300 μm $< c < 920\,\mu$m) lead to fracture toughness values in the regime: 6·2 MPa $\sqrt{m} < K_R < 8{\cdot}3$ MPa $\sqrt{m}$. Again, indentation-based fracture toughness measurements suffer from the complication that the attendant crack geometries exhibit relatively large CODs (compared to residual stress-free cracks). Therefore, too high a crack resistance for a relatively short (but wide) crack is obtained. Finally, a crack tip toughness, T_0, of 2·5 MPa $\sqrt{m}$, from a measurement of near crack tip ($x \approx 10\,\mu$m) opening displace-

ments,[25] was reported for SiC(w)/Al_2O_3. This value is close to the value determined ($T_0 = 2{\cdot}0$ MPa $\sqrt{m}$) for unreinforced alumina. Notwithstanding the rather low accuracy of this as yet novel technique ($\pm$20–30%), it is concluded, that whisker inclusions are effective primarily through crack bridging, not crack deflection.

5.2 Si_3N_4

A relatively high fracture toughness value for Si_3N_4 containing rod-shaped grains was reported by Lange almost 20 years ago.[31] Long crack *R*-curve measurements[32] in a DCB specimen start at a fracture toughness value of about 4·6 MPa $\sqrt{m}$. Indentation crack methods applied in similar materials give $K_R > 4{\cdot}3$ MPa $\sqrt{m}$ ($c > 50\,\mu$m), as reported by Li *et al.*,[33] while Ramachandran & Shetty[30] find $K_R > 7{\cdot}0$ MPa $\sqrt{m}$ ($c > 100\,\mu$m). These data can be compared to fracture toughness values obtained with materials with a K_R value of 1·8 MPa $\sqrt{m}$ for a fine-grained, pure Si_3N_4 and a K_A of 2·5 MPa $\sqrt{m}$ for a Si_3N_4 showing near 100% transgranular fracture. It should be pointed out that comparisons of data derived from different Si_3N_4 materials can only provide clues and no definite proof for toughening behavior of this material. In summary, it is yet unclear as to what toughening mechanism is responsible for raising a base fracture toughness value of about 2 MPa $\sqrt{m}$ to about 4 MPa $\sqrt{m}$ at a crack length around 50 μm. In analogy to SiC(w)/Al_2O_3, it is conjectured, however, that crack bridging is the dominant toughening mechanism in Si_3N_4.

6 Interaction between Crack Deflection and Crack Bridging

After the competitive nature of crack deflection and crack bridging have been expanded upon independently, attention is now directed to the interactive nature of both mechanisms. Two lines of arguments are possible.

The simple argument recognizes that an interaction between crack faces is only possible if the fracture surfaces are rough. Transgranular fracture with a continuous, uninterrupted fracture path has to be avoided. A rough crack face, however, is the consequence of crack deflection.

A more elaborate argument is based on a discussion of the activation of microstructural elements as crack bridges. Essentially all crack bridges[22] (elastic, plastic, elastic–plastic and ductile)

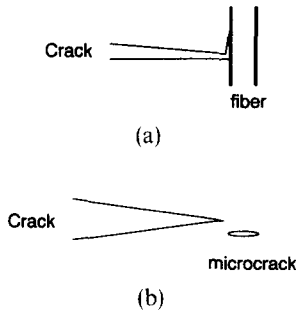

Fig. 6. Schematic for crack deflection (a) and crack deviation (b) from straight crack path.

require either crack deflection at the crack tip[5] ('strong reinforcement approach': Fig. 6(a)) or deviation of the crack from the straight crack path[22] ('residual stress approach': Fig. 6(b)). This requirement allows the set-up of the possible bridge geometries. Crack deflection with interface debonding[34] allows a reinforcing element to be strained to a sufficiently large degree such as to guarantee closure forces up to a large crack opening, u_0 (see eqn (4)). This requirement is in accordance with large bridging stresses acting over large distances away from the crack tip (eqn (2)). There is but one restriction to the argument that crack deflection plus debonding is required to guarantee large crack opening displacements around a reinforcement. This case comes in where ductile reinforcements do not debond at the matrix–ligament interface, but deform through cavitation (Fig. 3(d)). The large CODs around a bridging element are provided by an 'internal debonding mechanism' (crack/cavity formation) and attendant plastic flow. Crack deflection around the particle is then not required; the crack only needs to circumvent the ductile reinforcement (no twist or tilt).

Notwithstanding the complications coming in through the multitude of different bridge geometries, the generalizing and simplifying statement is provided: crack deflection is required for crack bridging.

7 Conclusions

The author has attempted to review some salient points in the theoretical and experimental work on crack deflection and crack bridging in ceramics over the last 15 years. It is concluded that crack deflection has a small potential as toughening mechanism compared to crack bridging. The development of methods to obtain reliable fracture toughness values, particularly for the crack tip toughness, T_0, is crucial to understand toughening and processing of tough ceramics. In particular, care has to be taken

where the crack resistance of short cracks with large COD (e.g. radial indentation cracks associated with a strong residual stress field) is evaluated. Measurements of crack opening displacements near the crack tip (and through the crack wake) are seen as very rewarding if one wishes to expand on potential toughening mechanisms. Crack path selection (crack deflection or deviation from the straight crack path) is shown to be crucial for bridge formation.

Acknowledgement

This work was supported by the Volkswagen Foundation under contract number I/66 790.

References

1. Evans, A. G. & Cannon, R. M., Toughening of brittle solids by martensitic transformations. *Acta Metall.*, **34** (1986) 761–800.
2. Rühle, M., Evans, A. G., McMeeking, R. M., Charalambrides, P. G. & Hutchinson, J. W., Microcrack toughening in alumina/zirconia. *Acta Metall.*, **35** (1987) 2701–10.
3. Mai, Y. W. & Lawn, B. R., Crack stability and toughness characteristics in brittle materials. *Ann. Rev. Mater. Sci.*, **16** (1986) 415–39.
4. Nickel H. & Steinbrech, R. W. (eds), *Mikrobruchvorgänge in Al_2O_3-Keramik*, Vol. 7, Forschungszentrum Jülich GmbH, 1991.
5. Faber, K. T. & Evans, A. G., Crack deflection processes—I. Theory. *Acta Metall.*, **31** (1983) 565–76.
6. Lawn, B. R., *Fracture of Brittle Solids*. Cambridge University Press, London, 1992.
7. Rice, J. R., Mathematical analysis in the mechanics of fracture. In *Fracture II*, ed. H. Liebowitz. Academic Press, New York, 1968.
8. Sneddon, I. N. & Lowengrub, M., *Crack Problems in the Classical Theory of Elasticity*. John Wiley and Sons, New York, 1969.
9. Borom, M. P., Turkalo, A. M. & Doremus, R. H., Strength and microstructure in lithium disilicate glass-ceramics. *J. Am. Ceram. Soc.*, **58** (1975) 385–91.
10. Faber, K. T. & Evans, A. W., Crack deflection processes—II. Experiment. *Acta Metall.*, **31** (1983) 577–84.
11. Evans, A. G., Perspective on the development of high-toughness ceramics. *J. Am. Ceram. Soc.*, **73** (1990) 187–206.
12. Becher, P. F., Microstructural design of toughened ceramics. *J. Am. Ceram. Soc.*, **74** (1991) 255–69.
13. Lange, F. F., Fracture mechanics and microstructural design. In *Fracture Mechanics of Ceramics*, Vol. 4, ed. R. C. Bradt, D. P. H. Hasselman & F. F. Lange. Plenum Press, New York, 1978, pp. 799–819.
14. Hübner, H. & Jillek, W., Sub-critical crack extension and crack resistance in polycristalline alumina. *J. Mat. Sci.*, **12** (1977) 117–25.
15. Knehans, R. & Steinbrech, R. W., Memory effect of crack resistance during slow crack growth in notched Al_2O_3 bend specimens. *J. Mat. Sci. Lett.*, **1** (1982) 327–9.
16. Knehans, R. & Steinbrech, R. W., Charakterisierung des subkritischen Bruchverhaltens reiner Al_2O_3-Keramiken. *Fortschrittsberichte der DKG*, **1**(3) (1985) 59–70.
17. Swanson, P. L., Fairbanks, C. J., Lawn, B. R., Mai, Y.-W. & Hockey, B. J., Crack-interface grain bridging as a fracture resistance mechanism in ceramics: I. Experimental study on alumina. *J. Am. Ceram. Soc.*, **70** (1987) 279–89.
18. Swanson, P. L., Crack-interface traction: a fracture-resistance mechanism in brittle polycrystals. In *Advances in Ceramics, Vol. 22, Fractography of Glasses and Ceramics*. American Ceramic Society, Columbus, OH, 1988, pp. 135–55.
19. Frei, H. & Grathwohl, G., Development of a piezo-translator-based bending device for in-situ SEM investigations of high-performance ceramics. *J. Phys. E: Sci. Instrum.*, **22** (1989) 589–93.
20. Vekinis, G., Ashby, M. F. & Beaumont, P. W. R., *R*-Curve behaviour of Al_2O_3 ceramics. *Acta Metall.*, **38** (1990) 1151–62.
21. Rödel, J., Kelly, J. F. & Lawn, B. R., In-situ measurements of bridged crack interfaces in the scanning electron microscope. *J. Am. Ceram. Soc.*, **73** (1990) 3313–18.
22. Rödel, J., Crack closure forces in ceramics: Characterization and formation. *J. Eur. Ceram. Soc.*, **9** (1992) 323–34.
23. Braun, L., Seidel, J. & Rödel, J., Crack opening displacement and residual stress of radial indentation cracks. *Acta Metall.*, submitted.
24. Haegerle, A. G., Cannon, W. R. & Denda, M., Direct measurement of crack tip stresses. *J. Am. Ceram. Soc.*, **74** (1991) 2897–901.
25. Rödel, J., Fuller, Jr, E. R. & Lawn, B. R., In-situ observations of toughening processes in alumina reinforced with silicon carbide whiskers. *J. Am. Ceram. Soc.*, **74** (1991) 3164–7.
26. Rödel, J., Sindel, M., Dransmann, M., Steinbrech, R. & Claussen, N., *R*-Curve behavior of metal reinforced ceramics. *J. Am. Ceram. Soc.*, submitted.
27. Jenkins, M. G., Kobayashi, A. S., White, K. W. & Bradt, R. C., Crack initiation and arrest in a SiC whisker/Al_2O_3 matrix composite. *J. Am. Ceram. Soc.*, **70** (1987) 393–5.
28. Krause, Jr, R. F. & Fuller, Jr, E. R., Fracture resistance behavior of silicon carbide whisker-reinforced alumina composites with different porosities. *J. Am. Ceram. Soc.*, **73** (1990) 559–66.
29. Homeny, J. & Vaughn, W. L., *R*-Curve behavior in a silicon carbide whisker/alumina matrix composite. *J. Am. Ceram. Soc.*, **73** (1990) 2060–2.
30. Ramachandran, N. & Shetty, D. K., Rising crack growth resistance (*R*-curve) behavior of toughened alumina and silicon nitride. *J. Am. Ceram. Soc.*, **74** (1991) 2634–41.
31. Lange, F. F., Relation between strength, fracture energy, and microstructure of hot-pressed Si_3N_4. *J. Am. Ceram. Soc.*, **56** (1973) 518–22.
32. Li, C.-W. & Yamanis, J., Super-tough silicon nitride with *R*-curve behavior. *Ceram. Eng. Sci.*, **10** (1990) 807–16.
33. Li, C.-W., Lee, D.-J. & Lui, S.-C., *R*-Curve behavior and strength for in-situ reinforced silicon nitrides with different microstructures. *J. Am. Ceram. Soc.*, submitted.
34. Charalambides, P. G. & Evans, A. G., Debonding properties of residually stressed brittle-matrix composites. *J. Am. Ceram. Soc.*, **72** (1989) 746–53.